

# Analytic Design of Sparse Rectangular Arrays for 3D Medical Ultrasound Imaging

Hansol Yoon  
Department of Electronic  
Engineering  
Sogang University  
Seoul, Korea, Republic of  
yoonhs@sogang.ac.kr

Sara Lee  
Department of Electronic  
Engineering  
Sogang University  
Seoul, Korea, Republic of  
dltkfk7812@sogang.ac.kr

Jeongyeon Kim  
Department of Electronic  
Engineering  
Sogang University  
Seoul, Korea, Republic of  
jenny0724@sogang.ac.kr

Tai-Kyong Song  
Department of Electronic  
Engineering  
Sogang University  
Seoul, Korea, Republic of  
tksong@sogang.ac.kr

**Abstract**—3D ultrasound imaging with 2D transducer arrays of large number of elements suffers from high hardware and computational complexity. In order to reduce the number of active channels, various sparse 2D array designs were presented. However, the proposed designs so far have either irregular element distribution that cannot guarantee uniformity among the scan lines or lack of analysis. In this study, a generalized sparse rectangular array (SRA) is presented, and a design rule that avoids common grating lobes of the transmit and receive SRA pairs is derived by analyzing the beam patterns. The continuous wave (CW) and pulsed wave responses of the SRA pairs are simulated to verify the proposed design rule.

**Keywords**—sparse 2D array, rectangular array, grating lobe, 3D ultrasound imaging

## I. INTRODUCTION

In 3D medical ultrasound imaging, ultrasound probes with 2D array transducers are used to effectively scan the imaging volume. Theoretically, dense 2D arrays having the interelement distance limited to half the acoustic wavelength are needed in order to avoid grating lobe artifacts. Such dense arrays usually require a huge number of elements, resulting in high hardware complexity. Also, the required speed for real-time imaging is hard to be met using large number of active elements since the computational cost is very high. Thus, designing sparse 2D arrays has been an important issue in realizing real-time 3D ultrasound imaging.

A problem with the sparse arrays is that they produce grating lobes in their beam patterns. There have been various design methods trying to overcome this problem. Undersampling elements randomly from a dense array is a reasonable approach to spread the grating lobe energy throughout the acoustic field [1]. This approach has been improved by optimization-theory-based approaches [2]-[4]. However, the sparse arrays designed by these methods cannot guarantee the uniformity among the scan lines because of their irregular distribution of elements. On the other hand, sparse periodic arrays, the so-called Vernier arrays, make use of the periodicity of the elements. By choosing the transmit and receive arrays with different periodicity, Vernier arrays suppress the grating lobes in the overall beam

pattern [5]-[8]. However, the general rule for choosing the transmit and receive periodic 2D arrays is not yet studied.

In this paper, a generalized model for sparse rectangular arrays (SRAs) is proposed, and a design rule for the transmit and receive SRA pairs (TRA/RRA) is derived by analyzing the beam patterns of the arrays. First, the far field, continuous wave (CW) response of an SRA is calculated analytically. Then the locations of the grating lobes are calculated to find the condition where the array pairs have common grating lobes (CGLs). Finally, the design rule for the array pairs that do not have CGLs is derived. Also, the near field, pulsed wave (PW) responses of the array pairs are simulated. Section II describes the derivation of the design rule, and Section III shows the CW and PW simulation results verifying the design rule. Conclusions are presented in Section IV.

## II. METHODS

### A. Sparse Rectangular Array (SRA)

Fig. 1 shows the model of sparse linear arrays (SLAs) that our group recently developed [9]. Here, the SLAs are generalized to SRAs (Fig. 2). An SRA is composed of  $N_{Px} \cdot N_{Py}$  subarray blocks, and in each subarray,  $L_x \cdot L_y$  elements are active out of  $P_x \cdot P_y$  elements. Such SRA is denoted as SRA- $L_x L_y$ . Using the coordinates of Fig. 3, the far field, CW response of an SRA,  $\Psi_{\text{SRA-}L_x L_y}(x, y, z)$ , can be factorized into  $x$  and  $y$  terms as

$$\Psi_{\text{SRA-}L_x L_y}(x, y, z) = \Psi_{\text{SLA-}L_x}(x, z) \cdot \Psi_{\text{SLA-}L_y}(y, z). \quad (1)$$

Given that  $u_x = x/R_0$  and  $u_y = y/R_0$ , (1) can be rewritten in spherical coordinates as

$$\Psi_{\text{SRA-}L_x L_y}(u_x, u_y) = \Psi_{\text{SLA-}L_x}(u_x) \cdot \Psi_{\text{SLA-}L_y}(u_y). \quad (2)$$

Since the response of an SLA,  $\Psi_{\text{SLA-}L}(u)$ , can be represented by the element factor  $\Phi_e(u)$ , the basic SLA factor  $\Psi_{\text{SLA-}1}(u)$  and the subarray factor  $\Psi_{\text{SA-}L}(u)$  [9], (2) can be represented as

$$\Psi_{\text{SRA-}L_x L_y}(u_x, u_y) \propto \Phi_e(u_x, u_y) \cdot \Psi_{\text{SLA-}1}(u_x, u_y) \cdot \Psi_{\text{SA-}L_x L_y}(u_x, u_y). \quad (3)$$

This work was supported by the R&D program of MOTIE/KEIT (10076675, Development of MR Based High Intensity Focused Ultrasound Systems for Brain and Urinogenital Diseases).

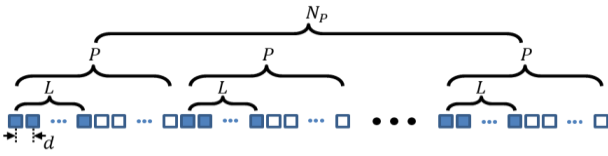


Fig. 1. Element layout scheme of a generalized SLA. In each subarray,  $L$  elements (colored) are active out of  $P$  elements.

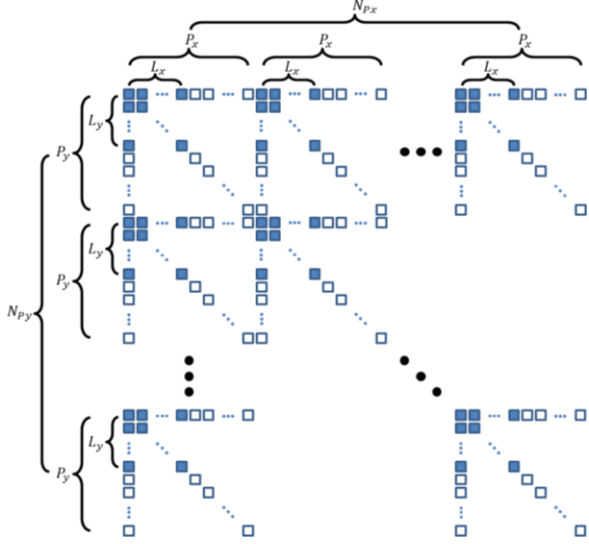


Fig. 2. 2D element layout of a generalized SRA.

Now the characteristics of (3) are examined by understanding the properties of  $\Psi_{\text{SLA-1}}(u_x, u_y)$  and  $\Psi_{\text{SA-L}_x\text{L}_y}(u_x, u_y)$ . Since

$$\Psi_{\text{SLA-1}}(u) = \frac{\sin(\pi N_P P d u / \lambda)}{\sin(\pi P d u / \lambda)}, \quad (4)$$

and

$$\Psi_{\text{SA-L}}(u) = \frac{\sin(\pi d L u / \lambda)}{\sin(\pi d u / \lambda)}, \quad (5)$$

where  $d$  is the element pitch, and  $\lambda$  is the acoustic wavelength, it is easy to show that  $\Psi_{\text{SRA-1}}(u_x, u_y)$  generates grating lobes in the locations of

$$(u_x, u_y) = \left( \frac{\lambda}{P_x d} \cdot m, \frac{\lambda}{P_y d} \cdot n \right), \quad (6)$$

$$0 < |m| < P_x d / \lambda, 0 < |n| < P_y d / \lambda, \text{ and } (m, n) \in \mathbb{Z}^2,$$

and  $\Psi_{\text{SA-L}_x\text{L}_y}(u_x, u_y)$  generates a null grid of

$$u_x = \frac{\lambda}{L_x d} \cdot m, u_y = \frac{\lambda}{L_y d} \cdot n, \quad (7)$$

$$0 < |m| < L_x d / \lambda, 0 < |n| < L_y d / \lambda, \text{ and } (m, n) \in \mathbb{Z}^2.$$

Also, the null-to-null main lobe width of  $\Psi_{\text{SRA-1}}(u_x, u_y)$  is calculated by (4) as  $2\lambda/N_P P d$ , which is equivalent to that of the corresponding dense array.

### B. Design Rule

The transmit and receive SRA pair (TRA/RRA) will be denoted by  $\text{TRA}(P_{x,T} \cdot P_{y,T}, L_{x,T} \cdot L_{y,T}) / \text{RRA}(P_{x,R} \cdot P_{y,R}, L_{x,R} \cdot L_{y,R})$  with the values of  $P$  and  $L$  in both  $x$  and  $y$  directions. The design rule is derived in order to avoid CGLs in the TRA/RRA pair. The grating lobes that share the same locations in both the transmit and receive beam patterns are said to be CGLs [9]. Since the grating lobes of the SRAs are present in the locations governed by (6) and (7), the locations of the CGLs are calculated as

$$(u_x, u_y) = \left( \frac{m}{m_0} \cdot \frac{\lambda}{d}, \frac{n}{n_0} \cdot \frac{\lambda}{d} \right), \quad (8)$$

$$0 < |m| < m_0 d / \lambda, 0 < |n| < n_0 d / \lambda, \text{ and } (m, n) \in \mathbb{Z}^2.$$

where  $m_0$  is the greatest common divider (GCD) of  $P_{x,T}$  and  $P_{x,R}$ , and  $n_0$  is the GCD of  $P_{y,T}$  and  $P_{y,R}$ .

With the knowledge of (8), the design rule for the array pair can be established. CGLs can be avoided by choosing the  $L$  values of

$$L_{x,R} = k_x \cdot m_0 \quad (9)$$

and

$$L_{y,R} = k_y \cdot n_0, \quad (10)$$

where  $k_x$  and  $k_y$  are natural numbers. One can easily show that a null grid of (7) that covers all the locations of the CGLs of (8) is formed with the parameters of (9) and (10). Thus by following the design rule, the grating lobes will be suppressed in the overall beam pattern of the TRA/RRA pair. Also, since the receive array already guarantees the CGL-cancelling null grid, the parameters of the transmit array,  $L_{x,T}$  and  $L_{y,T}$ , can be any natural numbers not greater than  $P_{x,T}$  and  $P_{y,T}$  respectively.

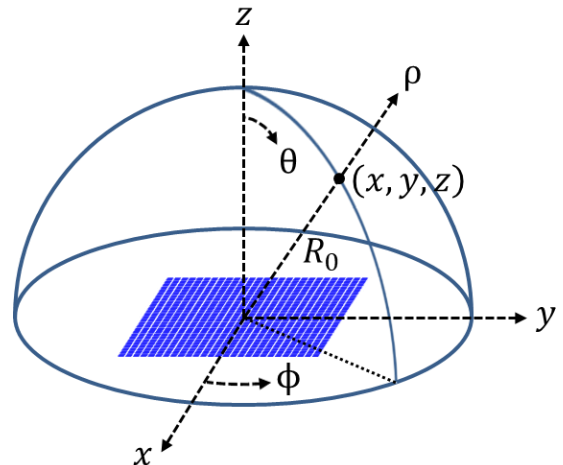


Fig. 3. Coordinate system for the theoretical and simulated beam patterns.

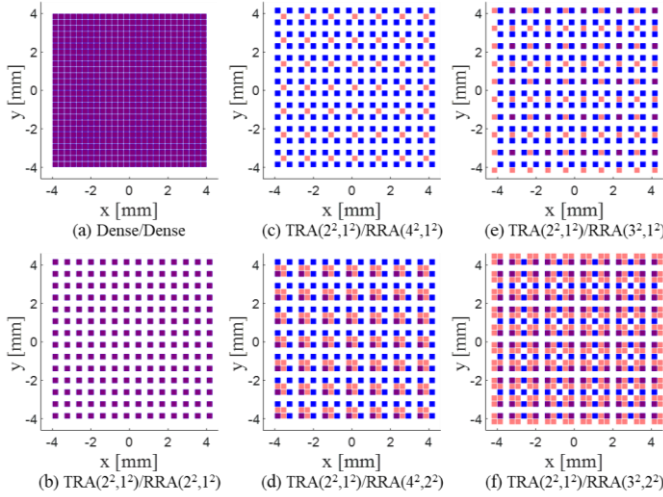


Fig. 4. TRA/RRA pairs used in the CW and PW simulations. Transmit elements are colored in blue, and receive elements are colored in red. Overlapping elements are colored in purple.

### III. SIMULATION RESULTS

#### A. Simulation Setup

Both CW responses and PW responses are calculated in a constant- $\rho$  hemispherical surface shown in Fig. 3. The CW

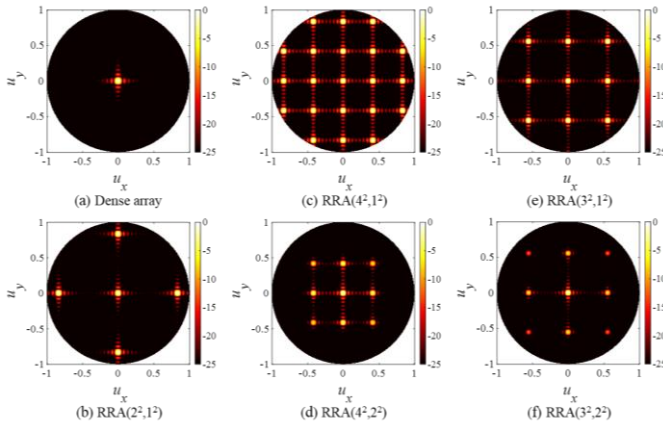


Fig. 5. One-way, CW responses of RRAs.

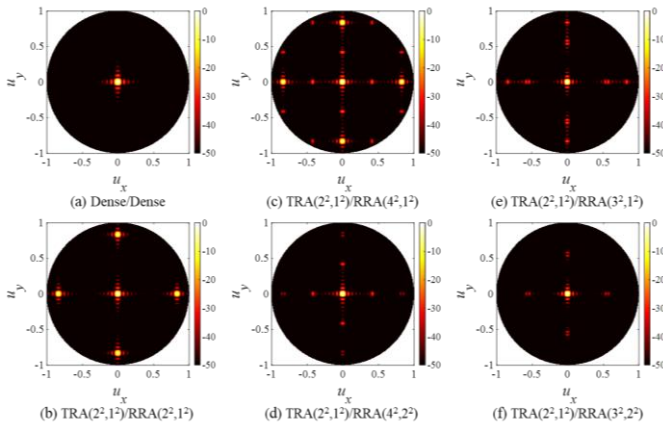


Fig. 6. Two-way, CW responses of SRA pairs.

responses are calculated by (3), and the PW responses are simulated by using Field II [10], [11]. The following parameters are used: sound speed of  $c = 1540$  m/s; central frequency of  $f_0 = 3$  MHz; sampling frequency of  $f_s = 100$  MHz; focal depth of  $F = 40$  mm; impulse response of a two-period sine with Hanning window; and a two-period sine excitation. Square-shaped elements are used with element width equal to  $0.5\lambda$  and the element pitch of  $0.6\lambda$ .

The array pairs used in the simulations are shown in Fig. 4. Except for the dense array pair (Fig. 4 (a)), the same TRA of  $\text{TRA}(2^2,1^2)$ , where  $P_{x,T} \cdot P_{y,T} = 2 \cdot 2 = 2^2$  and  $L_{x,T} \cdot L_{y,T} = 1 \cdot 1 = 1^2$ , is used in the array pairs. The dense array uses 676 ( $26 \times 26$ ) elements, whereas the  $\text{TRA}(2^2,1^2)$  uses 196 elements.  $\text{RRA}(2^2,1^2)$  uses exactly the same array as  $\text{TRA}(2^2,1^2)$ . Note that  $\text{RRA}(4^2,2^2)$  uses the same number of elements as  $\text{RRA}(2^2,1^2)$ . For the arrays  $\text{RRA}(3^2,1^2)$  and  $\text{RRA}(3^2,2^2)$ , 100 and 400 elements are activated respectively. The array pairs are grouped into the ones that do not follow the design rule (Fig. 4(b and c)) and the others that do follow the rule (Fig. 4(d to f)) by using different RRAs. The simulated responses of these array pairs were evaluated by their peak grating lobe level (PGL) and the mainlobe-to-sidelobe energy ratio (MSR) [1], [6], [7], [12].

#### B. CW and PW Responses

The one-way CW beam patterns of the receive arrays in Fig. 4 are shown in Fig. 5. For the dense array, only the main lobe is present in the beam pattern as shown in Fig. 5(a). On the other hand, the beam patterns of the RRAs have grating lobe patterns governed by (6) and (7). For example, the beam pattern of a  $\text{RRA}(4^2,2^2)$  (Fig. 5(d)) is the product of the beam pattern of a  $\text{RRA}(4^2,1^2)$  (Fig. 5(c)) and the null grid of  $u_x = \pm\lambda/2d$ ,  $u_y = \pm\lambda/2d$ . By comparing the beam patterns, it is clear that the  $\text{TRA}(2^2,1^2)/\text{RRA}(2^2,1^2)$  pair and the  $\text{TRA}(2^2,1^2)/\text{RRA}(4^2,1^2)$  pair have CGLs, but the pairs that follow the design rule,  $\text{TRA}(2^2,1^2)/\text{RRA}(4^2,2^2)$  pair, the  $\text{TRA}(2^2,1^2)/\text{RRA}(3^2,1^2)$  pair and the  $\text{TRA}(2^2,1^2)/\text{RRA}(3^2,2^2)$  pair, do not have CGLs as expected.

The effect of the CGLs are shown in the two-way CW beam patterns. Without following the design rule, the array pairs produce CGLs, resulting high grating lobes in the overall beam patterns (Fig. 6 (b and c)). In contrast, by following the design rule, the array pairs do not produce CGLs, thus the grating lobes

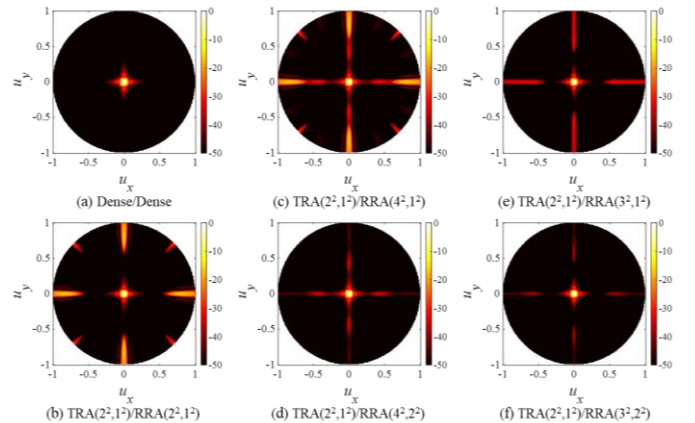


Fig. 7. Two-way, PW responses of SRA pairs.

are suppressed in the overall beam patterns as shown in Fig. 6(d to f). The same validation can be done with the PW responses shown in Fig. 7. The one notable difference is that the PW responses show relatively lower but broader grating lobes than the CW responses.

The profiles of the PW responses at  $u_y = 0$  are shown in Fig. 8 for comparison. Indeed, the array pairs designed by the rule have lower grating lobes than the  $\text{TRA}(2^2,1^2)/\text{RRA}(2^2,1^2)$  pair that do not follow the rule. For a quantitative comparison, the values of PGL/MSR of the designs that follow the rule are evaluated: -32.28 dB/16.15 dB for  $\text{TRA}(2^2,1^2)/\text{RRA}(3^2,1^2)$ ; -34.74 dB/21.21 dB for  $\text{TRA}(2^2,1^2)/\text{RRA}(4^2,2^2)$ ; and -38.52 dB/23.72 dB for  $\text{TRA}(2^2,1^2)/\text{RRA}(3^2,2^2)$ . On the other hand, for  $\text{TRA}(2^2,1^2)/\text{RRA}(2^2,1^2)$ , which does not follow the rule, the highest PGL and the lowest MSR of -15.96 dB/2.54 dB are measured. Note that the pair of  $\text{TRA}(2^2,1^2)/\text{RRA}(4^2,2^2)$  have much better performance than the  $\text{TRA}(2^2,1^2)/\text{RRA}(2^2,1^2)$  pair with the same number of elements used. Also, with the design rule followed, the more elements are used, the lower and the higher MSR are measured. In this study, the array pair of  $\text{TRA}(2^2,1^2)/\text{RRA}(3^2,2^2)$  has the best performance. By following the proposed design rule, SRA pairs can achieve comparable performance to that of the dense array pair (-41.94 dB/31.97 dB). Also, it is important to point out that the main lobe widths of the sparse array pairs are almost the same as that of the dense array pair as shown in Fig. 8.

#### IV. CONCLUSIONS

A generalized model of sparse periodic 2D arrays on a rectangular grid, namely SRAs, is presented. The beam patterns of the SRAs are calculated analytically in order to control the locations of the grating lobes. As a result, a design rule for CGL-free SRA pairs is developed. The design rule is then verified by the CW and PW simulation results. The results show that by following the rule, sparse 2D array pairs can be designed with comparable performances to that of the corresponding dense array using much less elements.

#### REFERENCES

[1] C. Boni, M. Richard and S. Barbarossa, "Optimal configuration and weighting of nonuniform arrays according to a maximum ISLR criterion," in *IEEE Int. Conf. Acoust., Speech, Sign. Proc.*, 1994, vol. 5, pp. 157-160.  
[2] J. W. Choe, O. Oralkan, and P. T. Khuri-Yakub, "Design optimization for a 2-D sparse transducer array for 3-D ultrasound imaging," in *Proc. IEEE Ultrason. Symp.*, 2010, pp. 1928-1931.

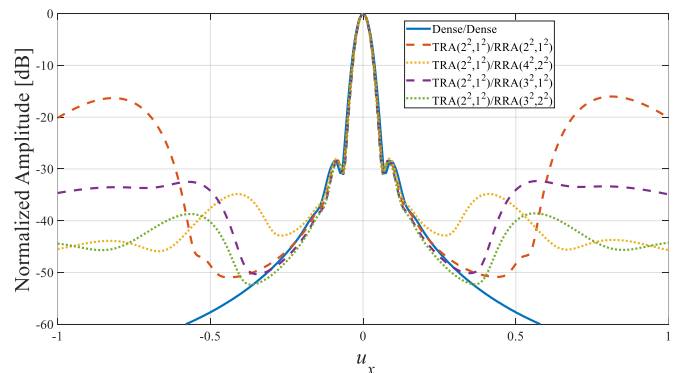


Fig. 8. 1D profile of the PW responses of the SRA pairs.

[3] B. Diarra, M. Robini, P. Tortoli, C. Cachard, and H. Liebgott, "Design of optimal 2-D nongrid sparse arrays for medical ultrasound," *IEEE Trans. Biomed. Eng.*, vol. 60, no. 11, pp. 3093-3102, Nov. 2013.  
[4] E. Roux, F. Varray, L. Petrusca, C. Cachard, P. Tortoli, and H. Liebgott, "Experimental 3-D ultrasound imaging with 2-D sparse arrays using focused and diverging waves," *Sci. Rep.*, vol. 8, no. 9108, pp. 1-12, 2018.  
[5] G. R. Lockwood and F. S. Foster, "Optimizing the radiation pattern of sparse periodic two-dimensional arrays," *IEEE Trans. Ultrason. Ferroelectr. Freq. Control*, vol. 43, no. 1, pp. 15-19, Jan. 1996.  
[6] S. I. Nikolov and J. A. Jensen, "Application of different spatial sampling patterns for sparse array transducer design," *Ultrasonics*, vol. 37, no. 10, pp. 667-671, 2000.  
[7] A. Austeng and S. Holm, "Sparse 2-D arrays for 3-D phased array imaging—Design methods," *IEEE Trans. Ultrason. Ferroelectr. Freq. Control*, vol. 49, no. 8, pp. 1073-1086, Aug. 2002.  
[8] A. Austeng and S. Holm, "Sparse 2-D arrays for 3-D phased array imaging—Experimental validation," *IEEE Trans. Ultrason. Ferroelectr. Freq. Control*, vol. 49, no. 8, pp. 1087-1093, Aug. 2002.  
[9] J. H. Song, J. Lee, S. Yeo, G. -D Kim and T. -K Song, "An analytical approach to designing optimal sparse 1D phased arrays for handheld ultrasound imaging," *IEEE Trans. Ultrason. Ferroelectr. Freq. Control*, submitted for publication.  
[10] J. A. Jensen and N. B. Svendsen, "Calculation of pressure fields from arbitrarily shaped, apodized, and excited ultrasound transducers," *IEEE Trans. Ultrason. Ferroelectr. Freq. Control*, vol. 39, no. 2, pp. 262-267, Mar. 1992.  
[11] J. A. Jensen, "Field: A program for simulating ultrasound systems," *Med. Biol. Eng. Comput.*, vol. 34, suppl. 1, pp. 351-353, 1996.  
[12] G. Oliveri and A. Massa, "ADS-based array design for 2-D and 3-D ultrasound imaging," *IEEE Trans. Ultrason. Ferroelectr. Freq. Control*, vol. 57, no. 7, pp. 1568-1582, Jul. 2010.